Available online at www.sciencedirect.com
ScienceDirect
Journal of Sound and Vibration 315 (2008) 746–765
JOURNAL OF SOUND AND VIBRATION
www.elsevier.com/locate/jsvi

Response regimes of linear oscillator coupled to nonlinear energy sink with harmonic forcing and frequency detuning

Y. Starosvetsky, O.V. Gendelman*

Faculty of Mechanical Engineering, Technion—Israel Institute of Technology, Haifa 32000, Israel

Accepted 19 December 2007
The peer review of this article was organised by the Guest Editor
Available online 19 February 2008

Abstract

Dynamical system under investigation in the current work is comprised of harmonically forced linear oscillator with attached nonlinear energy sink. External forcing frequency detuning near the main resonance (1:1) is included in the system investigation. The detailed study of the periodic and quasiperiodic regimes is done in the work via (adaptive) averaging method. Local bifurcations of the periodic regimes are revealed and fully described in the space of system parameters (amplitude of excitation, damping, and frequency detuning). Novel analytical approach for predictions of strongly modulated response (SMR) is presented. This approach provides a sufficient condition for the SMR existence contrary to the previous studies. Various possibilities of coexistence of the response regimes are predicted analytically and demonstrated numerically. Among those is a coexistence of two distinct periodic regimes together with the SMR. All findings of the simplified analytic model are verified numerically and considerable agreement is observed.

1. Introduction

Systems comprised of linear substructures with essentially nonlinear attachments are of great interest in a sense of vibration mitigation (in a linear substructure) and are intensively studied. Irreversible transient transfer (pumping) of energy from the substructure to the essentially nonlinear attachment (nonlinear energy sink (NES)) was demonstrated and studied in Refs. [1–4]. In the same papers, it has been shown that properly designed, essentially nonlinear local attachments may passively absorb energy from transiently loaded linear subsystems, acting as *NESs*. This obvious advantage of using essentially nonlinear attachments as NESs gave rise to an additional study of dynamics and performance of essentially nonlinear attachments coupled to the linear system substructure.

Addition of a relatively small and spatially localized nonlinear attachment leads to essential changes in the properties of the whole system. Unlike common linear and weakly nonlinear systems, systems with strongly nonlinear elements are able to react efficiently on the amplitude characteristics of the external forcing in a wide range of frequencies [4,5]. Thus, the systems under consideration give rise to a new concept of NES.

*Corresponding author. Tel.: +972 4 8293877; fax: +972 4 8295711.
E-mail address: ovgend@tx.technion.ac.il (O.V. Gendelman).

0022-460X/$ - see front matter © 2007 Elsevier Ltd. All rights reserved.
doi:10.1016/j.jsv.2007.12.023

It was demonstrated [2,3] that the possibility of the energy pumping phenomenon in non-conservative systems can be understood and explained by studying the energy dependence of the nonlinear undamped free periodic solutions (nonlinear normal modes (NNM)) of the corresponding conservative system which are obtained when all damping forces are eliminated. Recent investigation [6] based on the approach of invariant manifolds [7,8] has introduced an asymptotic procedure suitable for explicit inclusion of damping within the framework of NNM.

The steady-state response of the single-dof linear system with strongly nonlinear attachment to external forcing loading was studied in paper [9]. It was shown theoretically and experimentally that, in spite of weak coupling an essentially nonlinear attachment is capable of absorbing steady-state vibration energy from the linear oscillator, thus localizing the energy away from the directly forced subsystem. The energy absorption by strongly nonlinear attachment is realized over a relatively broad frequency range, making it effective over a range of frequencies.

In recent studies, it was demonstrated [10,11] that in close vicinity of the main resonance the system with NES can exhibit quasiperiodic rather than simple periodic response, leading to qualitatively different dynamical behavior. As it was shown in paper [11], strong mass asymmetry in periodically forced systems with essential nonlinearity may cause response regime qualitatively different from either simply periodic or weakly modulated regimes in the vicinity of 1:1 resonance. The former is characterized by very deep oscillations of the modulated amplitude comparable to the amplitude of the response itself. This response regime was considered in papers [11,12] and referred to as strongly quasiperiodic response. In fact, as it was demonstrated in Ref. [12] such response may be also phase locked or chaotic. In order to emphasize the difference of the response from simply periodic and weakly modulated quasiperiodic response, we use the term "strongly modulated response" (SMR). In the same paper [12], novel analytical approach was proposed for the SMR description. Possible effectiveness of the SMR was demonstrated in Ref. [13] from viewpoint of vibration absorption and mitigation compared with the best-tuned linear vibration absorber.

The goal of the present paper is an extensive study of the periodic and weakly quasiperiodic regimes, in a system comprised of the periodically forced linear oscillator coupled to the NES. Novel approach providing a sufficient condition for the SMR existence contrary to the previous studies is demonstrated. The main distinction of the current work from Refs. [10–13] is in extension of the considered system, namely in inclusion of the frequency detuning parameter near the main resonance in general treatment.

The structure of the paper is as follows. The second section is devoted to the brief model description. Section 3 brings a detailed study of the periodic solutions, their local bifurcations and also presents a novel approach for the SMR anticipation. Section 4 contains numerical verifications of the analytical model and also demonstrates various regimes coexistence predicted analytically. Section 5 contains concluding remarks and discussion.

2. Model

Analytical treatment of the model generally follows the analysis developed earlier [11] with modifications due to presence of the frequency detuning parameter.

The system considered in the paper is comprised of linear oscillator and strongly nonlinear attachment (pure cubic nonlinearity) and is forced harmonically. The system is described by the following equations:

$$\begin{aligned} &\ddot{y}_1 + \varepsilon\lambda(\dot{y}_1 - \dot{y}_2) + (1 + \varepsilon\sigma)y_1 + \tfrac{4}{3}\varepsilon(y_1 - y_2)^3 = \varepsilon A \cos t, \\ &\varepsilon\ddot{y}_2 + \varepsilon\lambda(\dot{y}_2 - \dot{y}_1) + \tfrac{4}{3}\varepsilon(y_2 - y_1)^3 = 0, \end{aligned} \tag{1}$$

where y_1 and y_2 are the displacements of the linear oscillator and the attachment, respectively, $\varepsilon\lambda$ is the damping coefficient, εA is the amplitude of external force and $\varepsilon\sigma$ is the frequency detuning parameter. $\varepsilon \ll 1$ is a small parameter, which establishes the order of magnitude for coupling, damping, amplitude of the external force, detuning parameter and mass of the attachment.

Coefficients A, λ, σ are adopted to be of order unity. Rigidity of the nonlinear spring is adopted to be equal to $4/3\varepsilon$. All the listed adoptions regarding system parameters do not affect a generality of a treatment below, since they may be changed independently by proper system rescaling.

3. Analytical treatment

3.1. Periodic solutions

In this section, we seek for the periodic solutions of Eq. (1) via averaging method used in Refs. [11,12]. Several changes of variables are applied on Eq. (1) for the sake of system simplification. The first change of variables is as follows:

$$v = y_1 + \varepsilon y_2, \quad w = y_1 - y_2. \tag{2}$$

Additional complex variables are introduced according to the following relationship:

$$\begin{aligned} \varphi_1 \exp(\mathrm{i}t) &= \dot{v} + \mathrm{i}v, \\ \varphi_2 \exp(\mathrm{i}t) &= \dot{w} + \mathrm{i}w. \end{aligned} \tag{3}$$

Introducing Eqs. (2), (3) into Eq. (1) and performing averaging procedure over one period of the external excitation the following slow modulated system is obtained:

$$\begin{aligned} &\dot{\varphi}_1 + \frac{\mathrm{i}\varepsilon}{2(1+\varepsilon)}(\varphi_1 - \varphi_2) - \frac{\mathrm{i}\varepsilon\sigma(\varphi_1 + \varepsilon\varphi_2)}{2(1+\varepsilon)} = \frac{\varepsilon A}{2}, \\ &\dot{\varphi}_2 + \lambda(1+\varepsilon)\frac{\varphi_2}{2} + \frac{\mathrm{i}}{2(1+\varepsilon)}(\varphi_2 - \varphi_1) - \frac{\mathrm{i}\varepsilon\sigma(\varphi_1 + \varepsilon\varphi_2)}{2(1+\varepsilon)} \\ &\quad - \frac{\mathrm{i}(1+\varepsilon)}{2}|\varphi_2|^2\varphi_2 = \frac{\varepsilon A}{2}. \end{aligned} \tag{4}$$

Fixed points of system (4) correspond to the periodic solutions of Eq. (1). In order to find the fixed points, we equate the derivatives of Eq. (4) to zero ($\dot{\varphi}_1 = \dot{\varphi}_2 = 0$) thus obtaining a system of complex algebraic equations:

$$\begin{aligned} &\frac{\mathrm{i}\varepsilon}{2(1+\varepsilon)}(\varphi_{10} - \varphi_{20}) - \frac{\mathrm{i}\varepsilon\sigma(\varphi_{10} + \varepsilon\varphi_{20})}{2(1+\varepsilon)} = \frac{\varepsilon A}{2}, \\ &\lambda(1+\varepsilon)\frac{\varphi_{20}}{2} + \frac{\mathrm{i}}{2(1+\varepsilon)}(\varphi_{20} - \varphi_{10}) - \frac{\mathrm{i}\varepsilon\sigma(\varphi_{10} + \varepsilon\varphi_{20})}{2(1+\varepsilon)} \\ &\quad - \frac{\mathrm{i}(1+\varepsilon)}{2}|\varphi_{20}|^2\varphi_{20} = \frac{\varepsilon A}{2}. \end{aligned} \tag{5}$$

By simple algebraic manipulations system of Eq. (5) may be reduced to a more convenient form

$$\begin{aligned} &\left[\lambda^2 + \frac{\sigma^2}{(1-\sigma)^2}\right]|\varphi_{20}|^2 + \frac{2\sigma}{1-\sigma}|\varphi_{20}|^4 + |\varphi_{20}|^6 = \frac{A^2}{(1-\sigma)^2}; \\ &\theta_{20} = \tan^{-1}\left(\frac{\sigma}{\lambda(1-\sigma)} + \frac{|\varphi_{20}|^2}{\lambda}\right) \\ &\varphi_{10} = \frac{(1+\varepsilon\sigma)\varphi_2 - i(1+\varepsilon)A}{1-\sigma} \\ &\Rightarrow |\varphi_{10}| = \frac{1+\varepsilon\sigma}{1-\sigma}\frac{|\varphi_{20}|\cos\theta_{20}}{\cos\theta_{10}} \\ &\theta_{10} = \tan^{-1}\left(\tan\theta_{20} - \frac{(1+\varepsilon)A}{(1+\varepsilon\sigma)|\varphi_{20}|\cos\theta_{20}}\right). \end{aligned} \tag{6}$$

Writing the first polynomial of Eq. (6) in a compact form yields

$$\alpha_1 Z + \alpha_2 Z^2 + \alpha_3 Z^3 + \alpha_4 = 0, \tag{7}$$

where

$$|\varphi_{20}|^2 = Z; \quad \alpha_1 = \lambda^2 + \frac{\sigma^2}{(1-\sigma)^2},$$
$$\alpha_2 = \frac{2\sigma}{(1-\sigma)}; \quad \alpha_3 = 1; \quad \alpha_4 = \frac{-A^2}{(1-\sigma)^2}.$$

Roots of polynomial (7) refer to the fixed points of Eq. (4) and thus to the periodic solutions of the original system (1).

3.2. Local bifurcations of the periodic solutions

In this section, we are going to investigate the local bifurcations of the periodic solutions obtained in Eq. (6).

3.2.1. Saddle-node bifurcation

In this part, we are going to find the boundary (cusp), which separates between zones of single real solution of Eq. (7) and three real solutions; this boundary corresponds to a saddle-node (SN) bifurcation. It is clear that the boundary of a SN bifurcation may be found by elimination of Z from Eq. (7) and the derivative of Eq. (7) equated to zero, thus providing necessary and complete conditions for the SN bifurcation:

$$3\alpha_3 Z^2 + 2\alpha_2 Z + \alpha_1 = 0. \tag{8}$$

Eliminating Z from Eqs. (7) and (8), one obtains the boundary of SN bifurcation in a space of (A, λ, σ) (ε—is fixed):

$$3\alpha_3(\alpha_1\alpha_2 - 9\alpha_3\alpha_4)^2 + 2\alpha_2(\alpha_1\alpha_2 - 9\alpha_3\alpha_4) \times(6\alpha_1\alpha_3 - 2\alpha_2^2) + \alpha_1(6\alpha_1\alpha_3 - 2\alpha_2^2)^2 = 0, \tag{9}$$

where α_1, α_2, α_3, and α_4 are defined in Eq. (7).

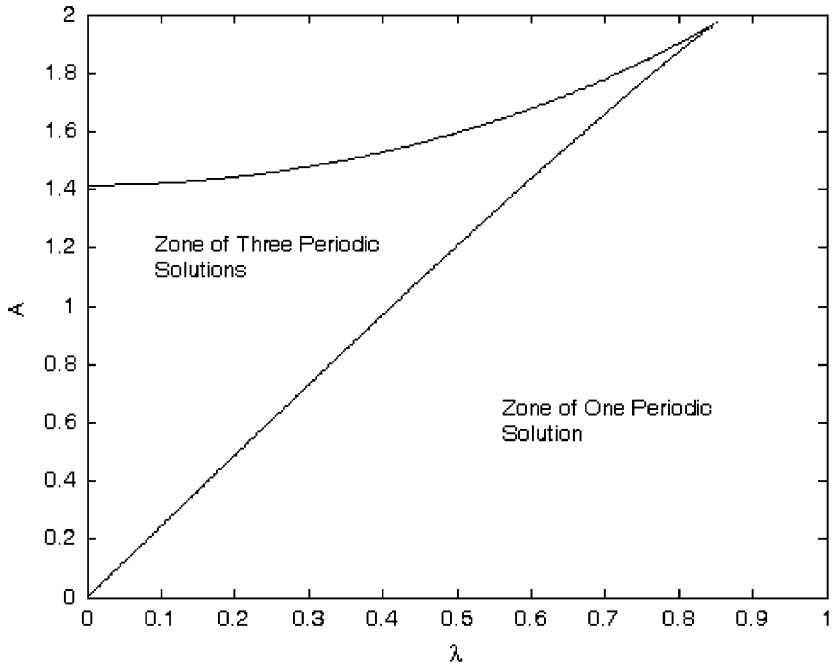

Fig. 1. Boundary of the SN bifurcation ($\sigma = 3$, $\varepsilon = 0.05$).

Therefore, Eq. (9) describes the boundary of the SN bifurcation, which separates between three periodic solutions to one. Projection of Eq. (9) to the two-dimensional plane of parameters (A, λ) for fixed value of σ is presented in Fig. 1.

Several projections for various positive and negative detuning (σ) values are plotted in Figs. 2 and 3.

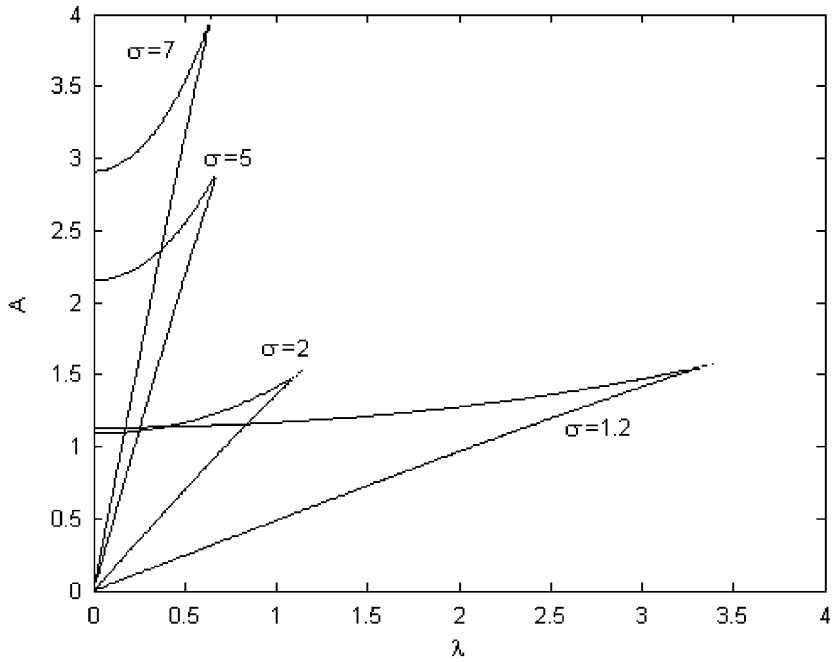

Fig. 2. Projections of the cusps of the SN bifurcation for the positive detuning values.

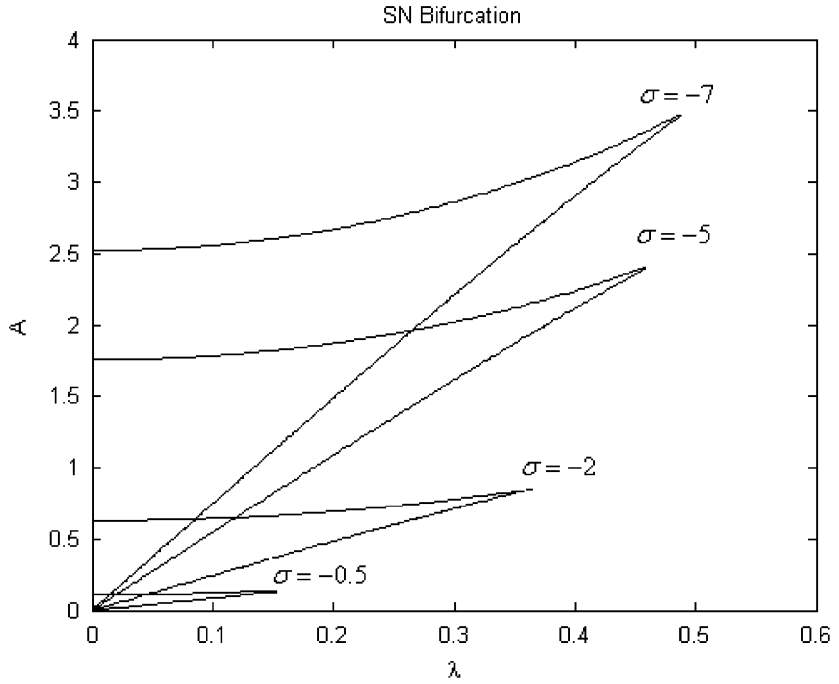

Fig. 3. Projections of the cusps of the SN bifurcation for the negative detuning values.

3.2.2. Hopf bifurcation

In order to explore the conditions for the Hopf bifurcation of the periodic solutions, we consider the small perturbations about the fixed points obtained in Eq. (6).

Small perturbation about the fixed point of the averaged system (4) is written in the following form:

$$\begin{aligned}\varphi_1 &= \varphi_{10} + \delta_1,\\ \varphi_2 &= \varphi_{20} + \delta_2,\end{aligned} \tag{10}$$

where the magnitudes of δ_1, δ_2 are of order ε. Substituting Eq. (10) into Eq. (4) and keeping the linear terms one obtains a linearized system:

$$\begin{aligned}\dot{\delta}_1 &= -\frac{\mathrm{i}\varepsilon}{2(1+\varepsilon)}(\delta_1-\delta_2)+\frac{\mathrm{i}\varepsilon\sigma(\delta_1+\varepsilon\delta_2)}{2(1+\varepsilon)}\\ \dot{\delta}_1^* &= \frac{\mathrm{i}\varepsilon}{2(1+\varepsilon)}(\delta_1^*-\delta_2^*)-\frac{\mathrm{i}\varepsilon\sigma(\delta_1^*+\varepsilon\delta_2^*)}{2(1+\varepsilon)}\\ \dot{\delta}_2 &= -\lambda(1+\varepsilon)\frac{\delta_2}{2}-\frac{\mathrm{i}}{2(1+\varepsilon)}(\delta_2-\delta_1)+\frac{\mathrm{i}\varepsilon\sigma}{2(1+\varepsilon)}(\delta_1+\varepsilon\delta_2)+\mathrm{i}(1+\varepsilon)\left|\varphi_{20}\right|^2\delta_2+\frac{\mathrm{i}(1+\varepsilon)}{2}\varphi_{20}^2\delta_2^*\\ \dot{\delta}_2^* &= -\lambda(1+\varepsilon)\frac{\delta_2^*}{2}+\frac{\mathrm{i}}{2(1+\varepsilon)}(\delta_2^*-\delta_1^*)-\frac{\mathrm{i}\varepsilon\sigma}{2(1+\varepsilon)}(\delta_1^*+\varepsilon\delta_2^*)-\mathrm{i}(1+\varepsilon)\left|\varphi_{20}\right|^2\delta_2^*-\frac{\mathrm{i}(1+\varepsilon)}{2}{\varphi_{20}^*}^2\delta_2.\end{aligned} \tag{11}$$

The characteristic polynomial of the linearized system (11) reads

$$\begin{aligned}&|\varphi_{20}| = N_{20},\\ &\gamma_1 = \lambda(1+\varepsilon),\\ &\gamma_2 = \left(\tfrac{3}{2}\varepsilon+\tfrac{3}{4}+\tfrac{3}{4}\varepsilon^3\right)N_{20}^4\\ &\qquad +(\varepsilon^2\sigma-1)N_{20}^2+\tfrac{1}{4}\lambda^2(\varepsilon+1)^2+\tfrac{1}{4}(\varepsilon^2\sigma^2+1),\\ &\gamma_3 = \tfrac{1}{4}\lambda\varepsilon(\varepsilon\sigma^2+1)\\ &\gamma_4 = \frac{3}{16}\varepsilon^2(1-\sigma)^2N_{20}^4+\tfrac{1}{4}\varepsilon^2\sigma(1-\sigma)N_{20}^2\\ &\qquad +\tfrac{1}{16}\varepsilon^2((1-\sigma)^2\lambda^2+\sigma^2),\\ &\text{The characteristic polynomial:}\\ &\mu^4+\gamma_1\mu^3+\gamma_2\mu^2+\gamma_3\mu+\gamma_4=0.\end{aligned} \tag{12}$$

The condition for the Hopf bifurcation requires the pair of pure imaginary eigenvalues:

$$\mu = \pm\mathrm{i}\Omega, \tag{13}$$

where Ω is real. Introducing Eq. (13) into characteristic polynomial obtained in Eq. (12) and splitting the expression into real and imaginary parts provides a condition for Hopf bifurcation and expression for Ω:

$$\begin{aligned}&\gamma_3^2-\gamma_2\gamma_3\gamma_1+\gamma_4\gamma_1^2=0,\\ &\Omega^2=\frac{\gamma_3}{\gamma_1}\Rightarrow\Omega=\pm\frac{1}{2}\sqrt{\frac{\varepsilon^2\sigma^2+\varepsilon}{1+\varepsilon}},\end{aligned} \tag{14}$$

where Ω refers to the frequency of modulation.

Expanding the first equation of Eq. (14) and collecting the powers of $z=N_{20}^2$, condition (14) reads

$$\begin{aligned}v_1 = &-\tfrac{3}{8}\varepsilon^4\sigma^2\lambda^2-\tfrac{3}{8}\varepsilon^2\sigma\lambda^2-\tfrac{3}{4}\varepsilon^3\sigma\lambda^2-\tfrac{3}{16}\lambda^2\varepsilon^5\sigma^2\\ &-\tfrac{3}{16}\lambda^2\varepsilon^3-\tfrac{3}{8}\varepsilon^4\sigma\lambda^2-\tfrac{3}{16}\lambda^2\varepsilon-\tfrac{3}{8}\lambda^2\varepsilon^2-\tfrac{3}{16}\varepsilon^3\sigma^2\lambda^2,\end{aligned}$$

$$
\begin{aligned}
v_2 &= \tfrac{1}{4}\lambda^2\varepsilon - \tfrac{1}{4}\lambda^2\varepsilon^4\sigma^3 - \tfrac{1}{4}\varepsilon^4\sigma^2\lambda^2 + \tfrac{1}{4}\varepsilon^2\sigma\lambda^2 \\
&\quad + \tfrac{1}{4}\varepsilon^3\sigma\lambda^2 - \tfrac{1}{4}\lambda^2\varepsilon^5\sigma^3 + \tfrac{1}{4}\lambda^2\varepsilon^2 - \tfrac{1}{4}\varepsilon^3\sigma^2\lambda^2, \\
v_3 &= \tfrac{1}{8}\varepsilon^3\sigma^2\lambda^2 - \tfrac{1}{16}\lambda^2\varepsilon - \tfrac{1}{8}\lambda^4\varepsilon^4\sigma - \tfrac{1}{16}\lambda^4\varepsilon^3 \\
&\quad - \tfrac{1}{16}\lambda^4\varepsilon - \tfrac{1}{8}\lambda^4\varepsilon^2 - \frac{1}{16}\lambda^2\varepsilon^5\sigma^4 - \tfrac{1}{8}\lambda^4\varepsilon^4\sigma^2 \\
&\quad - \tfrac{1}{16}\lambda^4\varepsilon^5\sigma^2 - \tfrac{1}{16}\lambda^4\varepsilon^3\sigma^2 - \tfrac{1}{8}\lambda^4\varepsilon^2\sigma - \tfrac{1}{4}\lambda^4\varepsilon^3\sigma,
\end{aligned} \tag{15}
$$

$$
v_1 z^2 + v_2 z + v_3 = 0 \text{ Condition for Hopf Bifurcation} \tag{16}
$$

It is obvious that solution of Eq. (16) should also satisfy Eq. (7), thus eliminating z from Eqs. (16) and (7) one obtains the boundary of stability for periodic solution:

$$
\begin{aligned}
z_1 &= \frac{\left(-v_2 - \sqrt{v_2^2 - 4v_3v_1}\right)}{2v_1}, \\
z_2 &= \frac{\left(-v_2 + \sqrt{v_2^2 - 4v_3v_1}\right)}{2v_1}.
\end{aligned} \tag{17}
$$

The boundaries of stability are

$$
\begin{aligned}
\alpha_1 z_1 + \alpha_2 z_1^2 + \alpha_3 z_1^3 + \alpha_4 = 0, \\
\alpha_1 z_2 + \alpha_2 z_2^2 + \alpha_3 z_2^3 + \alpha_4 = 0.
\end{aligned}
$$

The unstable region is bounded by these two curves. Projection of the boundary of stability (Hopf bifurcation) into the (A, λ) plane for the fixed values of σ and ε is drawn in Fig. 4.

By now, we have established the boundaries in the three dimensional space of parameters (A, λ, σ) for the SN and Hopf bifurcations. However, in the cases of more than one periodic solution there is an uncertainty in the determination of the particular bifurcating solution. In order to resolve the uncertainty, pairs of additional projections of bifurcation boundaries and bifurcation diagrams for the several detuning

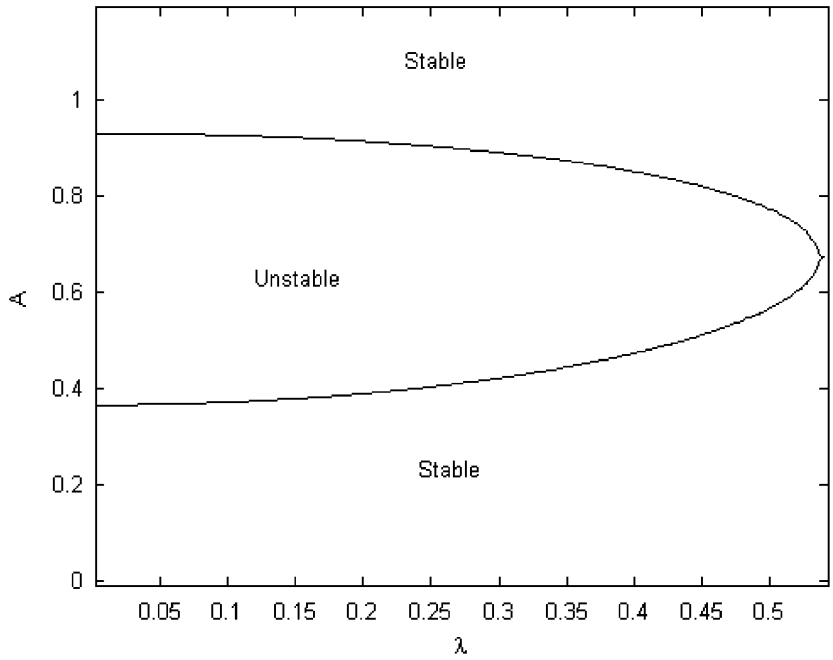

Fig. 4. Projection of the boundary of Hopf bifurcation ($\varepsilon = 0.05$).

values are demonstrated. By the term "bifurcation diagram" we imply the plot of the periodic solution amplitude (N_{20}) vs. external forcing amplitude (A). Thus, fixing the detuning (σ), damping (λ), and ε parameters we draw the diagrams marking on it the regions of bifurcations. The diagram presented in Fig. 5 relates to the projection shown in Fig. 4.

Additional pairs of the bifurcation boundary projections and bifurcation diagrams (for various values of σ) are brought in Figs. 6–9.

The results obtained in Figs. 4–9 require additional discussion. The diagram presented in Fig. 5 was constructed for $\sigma = 0.5$ (frequency detuning parameter value). Hopf bifurcation of the single periodic solution may be observed on the diagram of Fig. 5. The region within the boundary of Hopf bifurcation illustrated in Fig. 4 is unstable. Namely, it refers to the unstable periodic response solution. The region outside the boundary of Hopf bifurcation refers to the stable periodic response solution.

The boundary of Hopf bifurcation for $\sigma = 1.2$ depicted in Fig. 6 is fully occupied by the region of three periodic solutions due to SN bifurcation. In order to resolve the uncertainty regarding the Hopf bifurcation, namely to determine which of the periodic solutions bifurcates, a bifurcation diagram is plotted in Fig. 7.

It is clear from the diagram that the lower branch of the periodic solutions undergoes Hopf bifurcation for the fixed damping parameter ($\lambda = 0.2$). The obtained unstable region of the lower branch refers to the internal region of the Hopf bifurcation boundary presented in Fig. 6. The region of the SN bifurcation brought on the diagram as well, coincides with the internal region of the SN boundary (Fig. 6) for the fixed damping value ($\lambda = 0.2$).

The last case considered for $\sigma = 5$ differs from the previous cases in the type of Hopf bifurcation. As one can see in Figs. 8 and 9 crossing the lower branch of the Hopf bifurcation boundary (for $\lambda = 0.1$) (Fig. 8), we observe Hopf bifurcation of the middle unstable branch of the periodic solutions. which occurs at $A \approx 1.83$. Proceeding towards the growing values of external forcing amplitude (A) we face an additional Hopf bifurcation (Fig. 9) of the lower branch of periodic solutions for $A \approx 2$. This bifurcation occurs at the upper branch of the Hopf bifurcation boundary presented in Fig. 8 for the same value of damping parameter ($\lambda = 0.1$). Hopf bifurcation obtained for the last case brings qualitatively new kind of the loss of stability predicted by the boundaries of Fig. 8. Thus, the lower branch of the Hopf bifurcation boundary (Fig. 8)

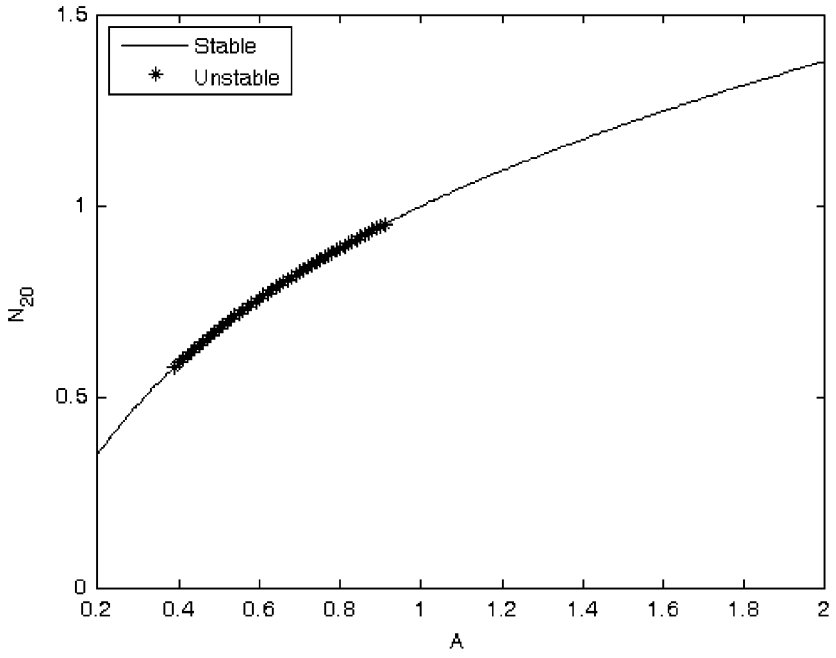

Fig. 5. Hopf bifurcation in a case of single periodic solution. ($\lambda = 0.2$, $\sigma = 0.5$, $\varepsilon = 0.05$). Additional pairs of the bifurcation boundary projections and bifurcation diagrams (for various values of σ) are brought in Figs. 6–9.

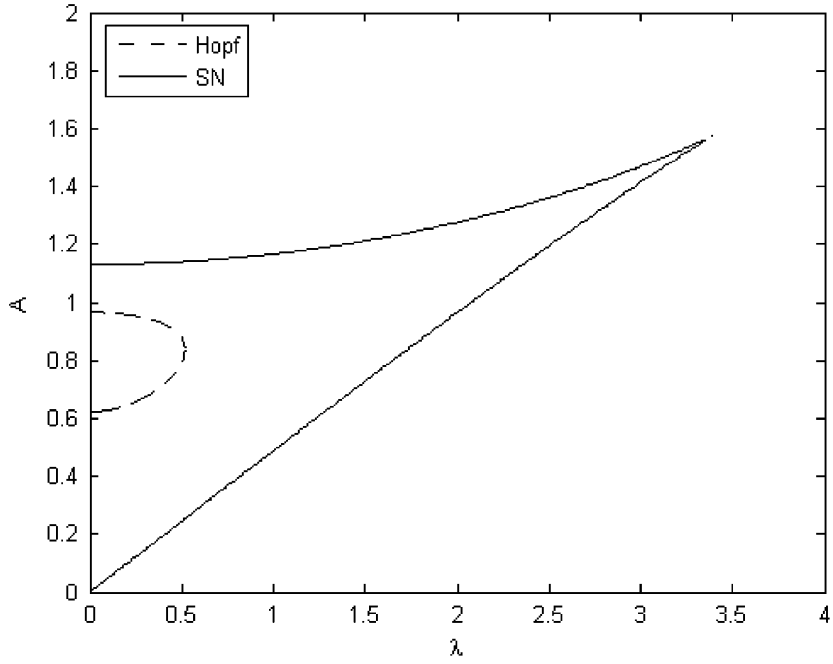

Fig. 6. Projection of the boundaries of Hopf and SN bifurcation lines ($\sigma = 1.2$, $\varepsilon = 0.05$).

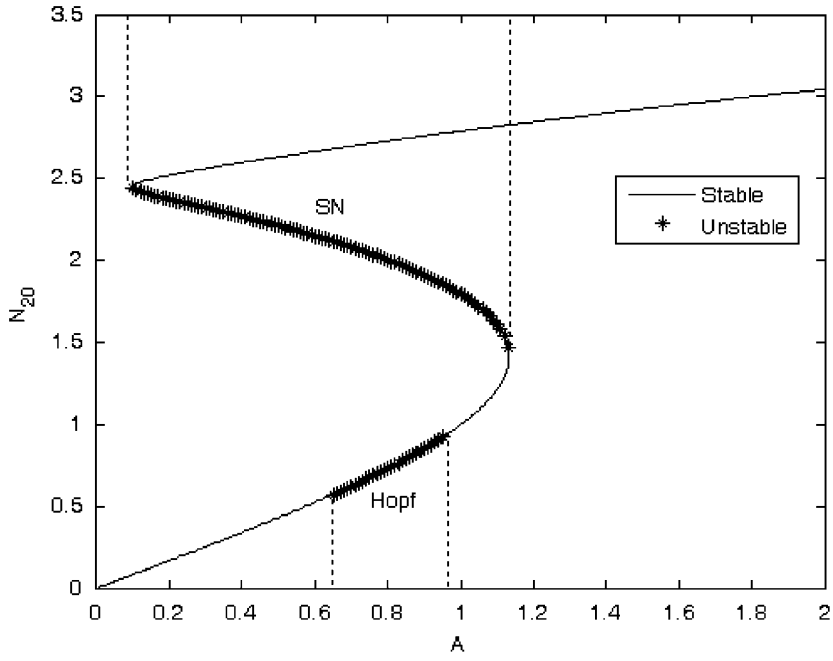

Fig. 7. Hopf and SN bifurcations diagram for fixed values of damping and detuning parameters.

depicts the bifurcation of the middle branch of the periodic solutions and the upper one depicts the bifurcation of the lower branch of periodic solutions. It is essential to note that the both branches are coalesce at the fold point ($A \approx 2.18$) and eventually vanish.

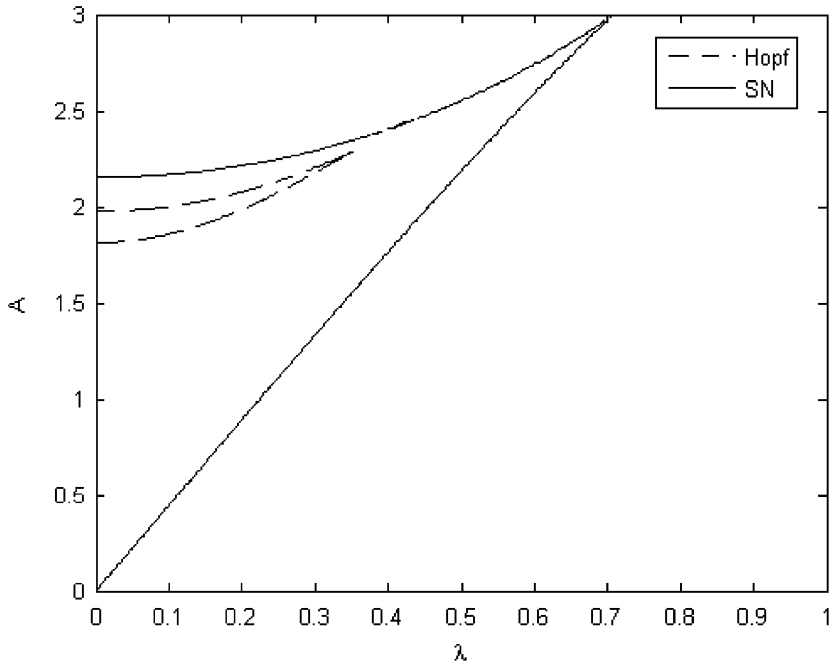

Fig. 8. Projection of the boundaries of Hopf and SN bifurcation lines on a two-dimensional plane ($\sigma = 1.2$, $\varepsilon = 0.05$).

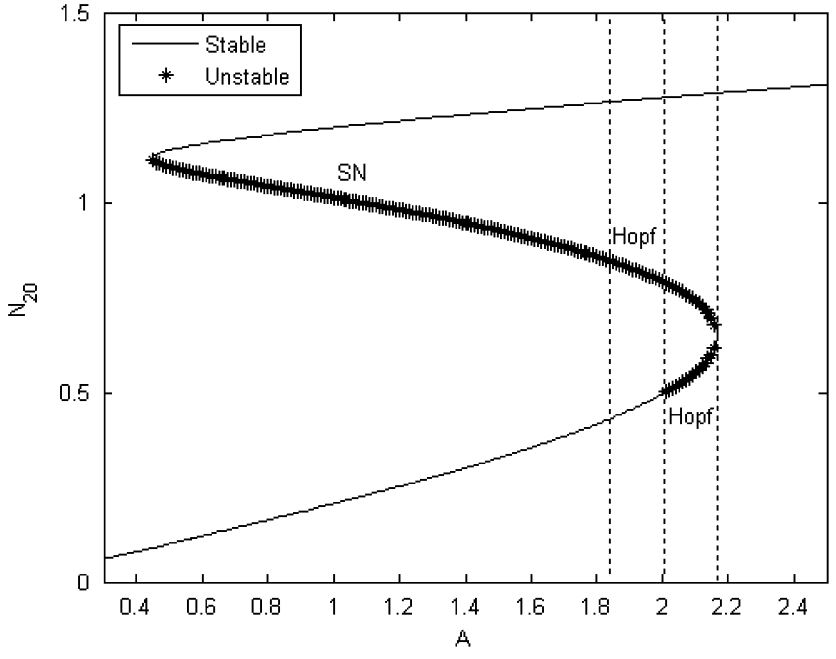

Fig. 9. Hopf and SN bifurcations diagram for the fixed values of damping and detuning parameters.

Another possibility to illustrate the local bifurcations of the periodic solutions is via frequency-response diagrams. Figs. 10–12 depict evolution of the frequency-response diagrams with growing values of the amplitude of excitation:

The points of bifurcations and their types are marked on the diagram. By observing the evolution of the frequency-response diagram one can note that there is a critical value of forcing amplitude ($A \approx 1$) Fig. 11 for

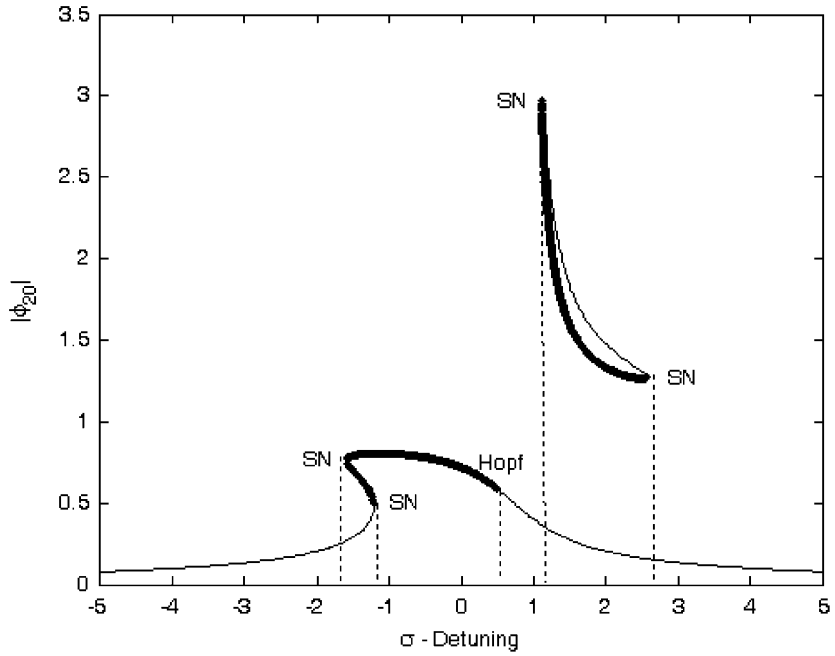

Fig. 10. Frequency-response diagram. Bold lines refer to the unstable regions of the periodic solutions when the thin lines refer to the stable regions. $A = 0.4$, $\lambda = 0.2$, $\varepsilon = 0.01$.

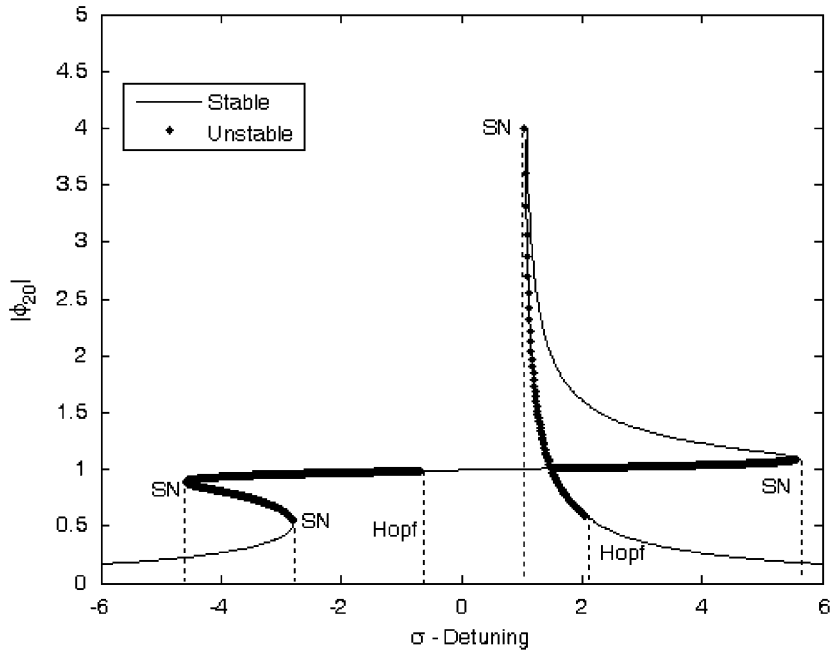

Fig. 11. Frequency-response diagram. Bold lines refer to the unstable regions of the periodic solutions when the thin lines refer to the stable regions. $A = 1.005$, $\lambda = 0.2$, $\varepsilon = 0.01$.

which the upper branch of the periodic responses coalesce with the lower one. For a slightly bigger value of forcing amplitude than a critical one ($A = 1.2$), the upper and lower curves are merged (Fig. 12). The diagrams accomplish the treatment of local bifurcations of the periodic solutions.

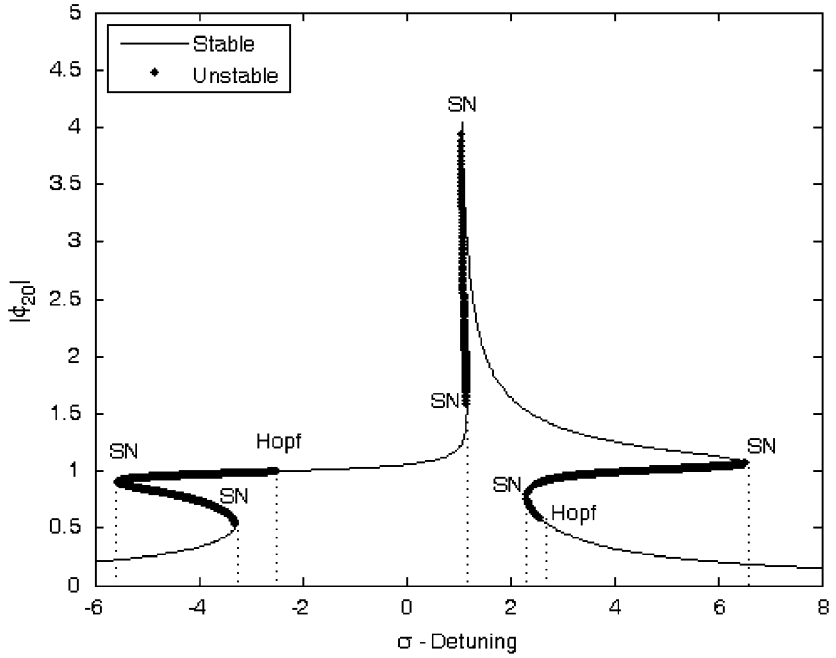

Fig. 12. Frequency-response diagram. Bold lines refer to the unstable regions of the periodic solutions when the thin lines refer to the stable regions. $A = 1.2$, $\lambda = 0.2$, $\varepsilon = 0.01$.

In the analysis performed above, we have observed 4 types of bifurcation mechanisms: SN bifurcation and generation of three periodic solutions, Hopf bifurcation of single periodic solution, Hopf bifurcation of one of the periodic solution in the region of three periodic solutions and finally Hopf bifurcation of two periodic solutions in the region of three solutions.

3.3. SMR

The analytical treatment of the previous section was concerned with the system periodic regimes. An extensive study of the local bifurcations of periodic regimes was performed and regions of stability and instability (in a space of parameters) were derived analytically. Additional, existing system response, which cannot be handled by the local analysis contrary to the simple periodic regimes is referred to as a SMR. As it comes from the previous studies [11–13], this response is characterized by the very deep modulation of the oscillations and has amplitude comparable to the response itself.

In paper [13], it was demonstrated numerically that the SMR exists in the vicinity of the exact 1:1 resonance and may be very favorable from the viewpoint of vibration absorption and mitigation (better than tuned linear absorber). However, these results were not complete—the analytic method developed in Ref. [13] allowed finding only necessary conditions for the SMR in the conditions of exact resonance.

In this section, we describe an analytical approach providing one a sufficient condition for the existence of SMR.

By simple manipulations, system (4) may be reduced to single second-order ODE:

$$\begin{aligned}\frac{\mathrm{d}^2\varphi_2}{\mathrm{d}t^2} &+ \frac{\mathrm{d}}{\mathrm{d}t}\left[\alpha\varphi_2 - \frac{\mathrm{i}(1+\varepsilon)}{2}|\varphi_2|^2\varphi_2 + \frac{\mathrm{i}\varepsilon}{2(1+\varepsilon)}(1-\sigma)\varphi_2\right] \\ &+ \frac{\mathrm{i}\varepsilon}{2(1+\varepsilon)}(1-\sigma)\left[\alpha\varphi_2 - \frac{\mathrm{i}(1+\varepsilon)}{2}|\varphi_2|^2\varphi_2 - \frac{\varepsilon A}{2}\right] \\ &- \frac{\mathrm{i}\varepsilon\beta}{2(1+\varepsilon)}[1+\varepsilon\sigma]\varphi_2 = \frac{\varepsilon A\beta}{2}, \end{aligned} \tag{18}$$

where

$$\alpha = \frac{\lambda(1+\varepsilon)^2 + \mathrm{i} - \mathrm{i}\varepsilon^2\sigma}{2(1+\varepsilon)}, \quad \beta = \frac{\mathrm{i}}{2(1+\varepsilon)}(1+\varepsilon\sigma).$$

Multiple-scale expansion is introduced as

$$\varphi_2 = \varphi_2(\tau_0, \tau_1, \ldots), \quad \frac{\mathrm{d}}{\mathrm{d}t} = \frac{\partial}{\partial\tau_0} + \varepsilon\frac{\partial}{\partial\tau_1} + \cdots,$$
$$\tau_k = \varepsilon^k t, \; k = 0, 1, \ldots . \tag{19}$$

Substituting Eq. (19) into Eq. (18) and equating the like powers of ε one obtains equations for zero and the first-order approximations:

$$\varepsilon^0 : \frac{\partial^2\varphi_2}{\partial\tau_0^2} + \frac{\partial}{\partial\tau_0}\left[\frac{\lambda\varphi_2}{2} + \frac{\mathrm{i}\varphi_2}{2} - \frac{\mathrm{i}}{2}|\varphi_2|^2\varphi_2\right] = 0,$$
$$\varepsilon^1 : 2\frac{\partial^2\varphi_2}{\partial\tau_0\partial\tau_1} + \frac{\partial}{\partial\tau_1}\left[\frac{\lambda\varphi_2}{2} + \frac{\mathrm{i}\varphi_2}{2} - \frac{\mathrm{i}}{2}|\varphi_2|^2\varphi_2\right]$$
$$+ \frac{\partial}{\partial\tau_0}\left[\frac{\lambda\varphi_2}{2} + \frac{\mathrm{i}(1-\sigma)\varphi_2}{2} - \frac{\mathrm{i}}{2}|\varphi_2|^2\varphi_2\right]$$
$$+ \frac{1-\sigma}{4}|\varphi_2|^2\varphi_2 + \left[\frac{\sigma}{4} + \frac{\mathrm{i}\lambda(1-\sigma)}{4}\right]\varphi_2 - \frac{\mathrm{i}A}{4} = 0. \tag{20}$$

The first equation of Eq. (20) describes "fast" evolution of the averaged system. It can be trivially integrated:

$$\frac{\partial}{\partial\tau_0}\varphi_2 + \left(\frac{\mathrm{i}}{2}\varphi_2 + \frac{\lambda}{2}\varphi_2 - \frac{\mathrm{i}}{2}|\varphi_2|^2\varphi_2\right) = C(\tau_1, \ldots), \tag{21}$$

where C is arbitrary function of higher-order time scales. Approximations of higher orders are not used in current analysis. Then for the sake of brevity only dependence on time scales τ_0 and τ_1 will be denoted explicitly below. Fixed points $\Phi(\tau_1)$ of Eq. (21) depend only on time scale τ_1 and obey algebraic equation:

$$\frac{\mathrm{i}}{2}\Phi + \frac{\lambda}{2}\Phi - \frac{\mathrm{i}}{2}|\Phi|^2\Phi = C(\tau_1). \tag{22}$$

Eq. (22) is easily solved by taking $\Phi(\tau_1) = N(\tau_1)\exp(\mathrm{i}\theta(\tau_1))$ and performing simple calculations:

$$\lambda^2 N^4 + (N^2 - N^4)^2 = 4|C(\tau_1)|^2 N^2$$

or equivalently

$$\lambda^2 Z(\tau_1) + Z(\tau_1)(1 - Z(\tau_1))^2 = 4|C(\tau_1)|^2,$$
$$Z(\tau_1) = (N(\tau_1))^2. \tag{23}$$

Expression for argument of the fixed point may be written as

$$\theta(\tau_1) = \arg C(\tau_1) - \tan^{-1}\frac{1 - Z(\tau_1)}{\lambda}, \tag{24}$$

where $Z(\tau_1)$ is solution of Eq. (23).

The number of solutions of Eq. (23) depends on $|C(\tau_1)|$ and λ. The function in the left-hand side can be monotonous or have maximum and minimum. In the former case, the change of $|C(\tau_1)|$ has no effect on the number of solutions—Eq. (23) will have one positive solution. In the latter case, the change of $|C(\tau_1)|$ will bring about a pair of SN bifurcations. In order to distinguish between different cases, we should check whether the derivative of the left-hand side of Eq. (21) has roots:

$$1 + \lambda^2 - 4Z + 3Z^2 = 0 \quad \text{or} \quad Z_{1,2} = \frac{2 \pm \sqrt{1 - 3\lambda^2}}{3}. \tag{25}$$

Therefore, two roots and pair of SN bifurcations exist for $\lambda<1/\sqrt{3}$ and do not exist otherwise. At critical value, $\lambda=1/\sqrt{3}$ two SN bifurcation points coalesce, thus forming a typical structure of a cusp catastrophe.

It is easy to see from Eq. (21) if only one solution of Eq. (23) exists, it is stable with respect to time scale τ_0. If there are three solutions, two of them are stable (nodes) and one unstable (saddle). Therefore, at time scale τ_0 the phase point will be attracted to one of the nodes. In fact, Eq. (22) defines slow invariant manifold (SIM) of the problem. In the case $\lambda<1/\sqrt{3}$ the fold lines $N(\tau_1)=Z_{1,2}^{1/2}, \quad \theta(\tau_1)\in(0,2\pi)$ divide stable and unstable branches of the SIM. Fig. 13 demonstrates projection of the two-dimensional SIM on the plane (N, C), the fold lines correspond to the points of maximum and minimum.

It is well-known [14,15] that such structure of the SIM may give rise to relaxation-type oscillations of the system (the hypothetic "jumps" between the stable branches are denoted by arrows in Fig. 13). Still, such motion is possible only if the system can reach the fold lines while moving on the SIM with respect to the slow time scale. In order to assess this possibility, one should investigate the behavior of $\Phi(\tau_1)$. For this sake, we consider the ε^1 term of multiple-scale expansion namely the second equation of Eq. (20). We are interested in the behavior of the solution on the stable branches of the SIM $\Phi(\tau_1)=\lim_{\tau_0\to+\infty}\varphi_2(\tau_0,\tau_1)$. Taking the limit $\tau_0\to\infty$ in the second equation of system (20) and taking into account the asymptotic stability of the points of the stable branches with respect to time scale τ_0, one obtains

$$\frac{\partial}{\partial\tau_1}\left[\frac{\lambda\Phi}{2}+\frac{\mathrm{i}\Phi}{2}-\frac{\mathrm{i}}{2}|\Phi|^2\Phi\right]+\frac{1-\sigma}{4}|\Phi|^2\Phi+\left[\frac{\sigma}{4}+\frac{\mathrm{i}\lambda(1-\sigma)}{4}\right]\Phi-\frac{\mathrm{i}A}{4}=0. \tag{26}$$

Eq. (26) can be written in the more convenient form:

$$\left[\frac{\lambda}{2}+\frac{\mathrm{i}}{2}-\mathrm{i}|\Phi|^2\right]\frac{\partial\Phi}{\partial\tau_1}-\frac{\mathrm{i}}{2}\Phi^2\frac{\partial\Phi^*}{\partial\tau_1}=G$$
$$G=-\frac{1-\sigma}{4}|\Phi|^2\Phi-\left[\frac{\sigma}{4}+\frac{\mathrm{i}\lambda(1-\sigma)}{4}\right]\Phi+\frac{\mathrm{i}A}{4}. \tag{27}$$

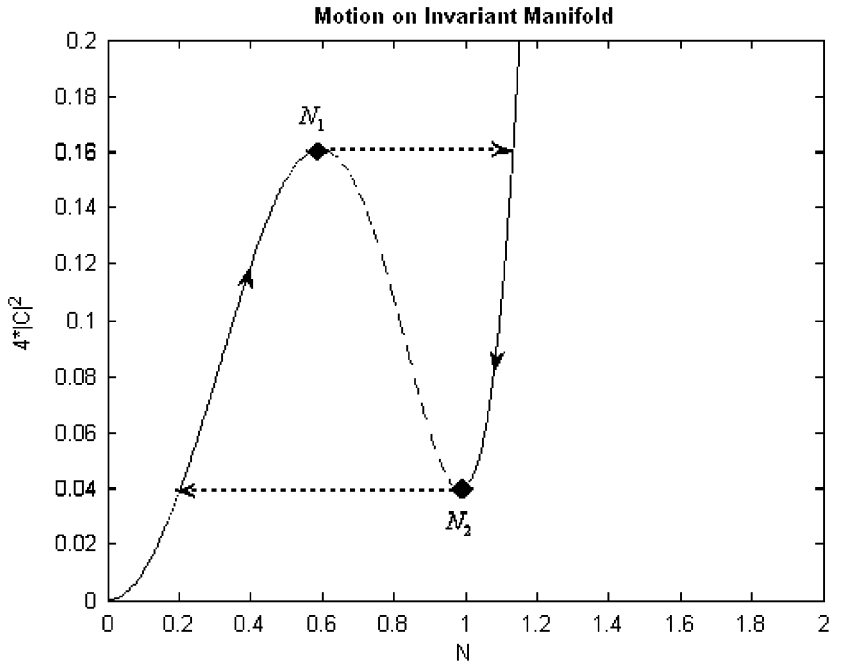

Fig. 13. Projection of the slow invariant manifold of the system in accordance with Eq. (33), $\lambda=0.2$. The unstable branch is denoted by dashed line. Arrows denote hypothetic jumps in the regime of the relaxation oscillations.

By taking complex conjugate of Eq. (27), it is possible to extract the derivative $\partial\Phi/\partial\tau_1$:

$$\frac{\partial\Phi}{\partial\tau_1}=\frac{2[(\lambda-\mathrm{i}+2\mathrm{i}|\Phi|^2)G+\mathrm{i}\Phi^2G^*]}{\lambda^2+1-4|\Phi|^2+3|\Phi|^4}. \tag{28}$$

System presented in Eq. (28) describes dynamics on the stable branches of the SIM. Results obtained in the present analysis as it was demonstrated in Eq. (28) make it possible to depict the SMR via one-dimensional maps. We will briefly repeat the main results of Eq. (28) and as an example will construct the one-dimensional map depicting the SMR in the limit $\varepsilon\to 0$. We start with the phase portrait constructed for the slow evolved system (28) (Fig. 14).

Observing the phase portrait presented in Fig. 14, one can easily notice that there are phase trajectories on either low stable branch or upper one, which reach the folds. These trajectories actually allow the existence of SMR. However, it is quite obvious that an existence of these trajectories on each stable branch of SIM cannot guarantee the stability of the SMR. The reason for that is a possibility of the SMR to be attracted to another stable response (e.g. simple periodic) after several jumps from one stable branch to another. In order to track the stability of the SMR response and thus to allow the tools for prediction of its existence one-dimensional maps are constructed. Observing the phase portrait presented in Fig. 14 we can see that there is an interval of $\theta-[\Theta_1<\theta<\Theta_2]$ for which all the phase trajectories are repelled from the lower fold N_1 ($|\Phi|=N_1$). In the regime of the relaxation oscillations, the phase trajectory jumps from a point of this interval to the upper branch of the SIM, then it moves along the line of the slow flow to the upper fold line, then jumps back to the lower branch and moves to the lower fold line, commencing in one of the points of the interval $[\Theta_1,\ \Theta_2]$ in order to enable the next jump. Therefore, it is natural to consider this regime as mapping of the interval $[\Theta_1,\ \Theta_2]$ into itself—the regime of the relaxation oscillations will correspond to attractor of this one-dimensional map. Existence of this attractor is therefore necessary and sufficient condition for existence of the SMR for system (4), or, equivalently, Eq. (18), when the mass ratio ε is small enough.

In order to build the relevant mapping, we should consider separately the "slow" and the "fast" parts of the mapping cycle. As for the "slow" parts on the lower and the upper branches of the SIM, we can use Eq. (28) and directly connect the "entrance" and "exit" points. Owing to the complexity of the equations, this part of the mapping should be accomplished numerically. As for the "fast" parts, the function φ_2 should be

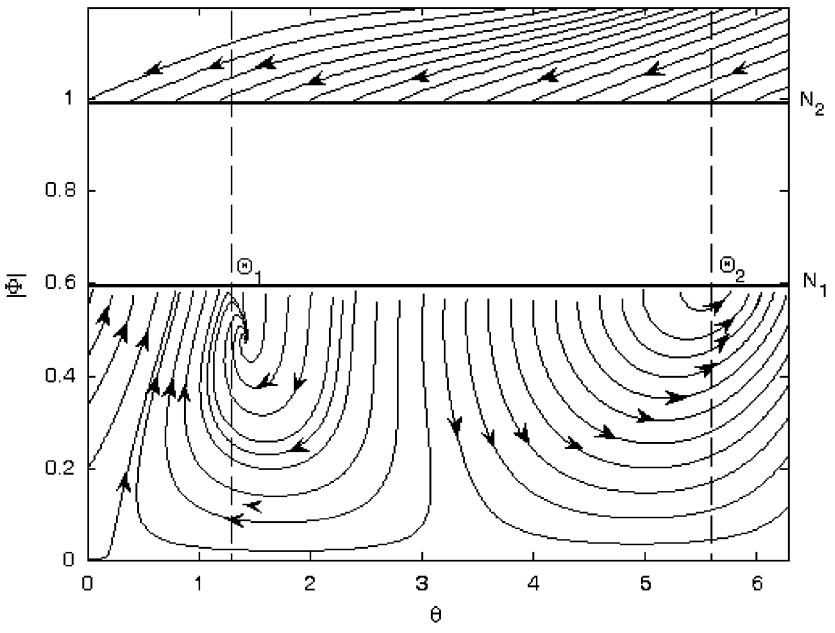

Fig. 14. Phase portrait of the slow invariant manifold (only stable branches of the SIM are shown).

continuous at the points of contact between the "fast" and the "slow" parts. Therefore, for "fast" parts of the motion one obtains complex invariant $C(\tau_1)$, defined by Eq. (22). If one knows its value at the point of "start", it is possible to compute N and θ for the point of "finish" unambiguously and thus to complete the mapping. The procedure of numerical integration should be performed twice—for two branches of the SIM. Two invariants should be computed for two "fast" jumps, in order to determine their final points. It should be stressed that only one computation cycle of the mapping for each point of the initial interval is required. This idea of mapping is close to that used in paper [14] for analysis of chaotic attractors of the relaxation oscillations in the state space of lower dimensionality.

Not every trajectory which starts from the lower fold of the SIM will reach the initial interval since it may be attracted to alternative attractor at the upper or the lower branch of the SIM, if it exists. Of course, only those points, which are mapped into the interval can carry sustained relaxation oscillations. The mapping procedure is illustrated in Figs. 15 and 16.

The mapping in Fig. 15 exists for all points of the interval and is obviously contractive; therefore one can expect existence of stable attractor corresponding to the regime of the relaxation oscillations (or SMR). In this case, it is single-period cycle originating at a point $\theta \approx 0.51$. By increasing the detuning parameter value (the values of the forcing amplitude and the damping parameters remain the same), one can notice the changes that mapping diagram undergoes (Fig. 16). As it comes from the diagram (Fig. 16), all the mapping lines tend to the right and there is also a region on the basin, which does not contain any lines. This region relates to the unaccomplished cycles, namely to the phase trajectories which started from the region and have been attracted to the periodic response attractor before they have reached the basin once more. The mentioned trajectories are not illustrated on the diagram. Thus, the empty regions of basin on the diagrams will be related to the trajectories, which do not reach the basin once more. It is clear from Fig. 16 that there is no stable attractor of the SMR and for every initial condition on the basin the system finally (after sufficient number of cycles) leaves the basin. Consequently, the relaxation oscillations will exist in transient response under certain initial conditions, but not in the sustained response. Such situation requires presence of alternative attractor.

By now we can conclude that for some increased values of detuning parameter the SMR attractor vanishes.

Running with the values of detuning (σ) and for each step performing the mapping one can track the value of σ for which the attractor vanishes. This provides a general tool for determination of the frequency region for the existence of SMR. For current system, the boundaries of the detuning parameter within which the SMR exists are $\sigma_R = 2.69 > \sigma > \sigma_L = -2.0546$. So, as it was established earlier by direct numerical simulation, the SMR exists in rather small vicinity of the exact 1:1 resonance.

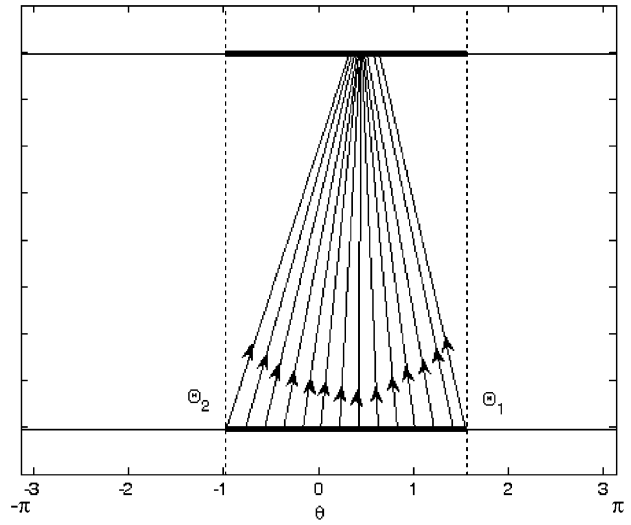

Fig. 15. One-dimensional mapping: $\sigma = -0.5$, $A_1 = 0.6$, $\lambda = 0.2$. Horizontal bold lines refer to the basin of jump $\Theta_1 < \theta < \Theta_2$, arrows denote direction of mapping.

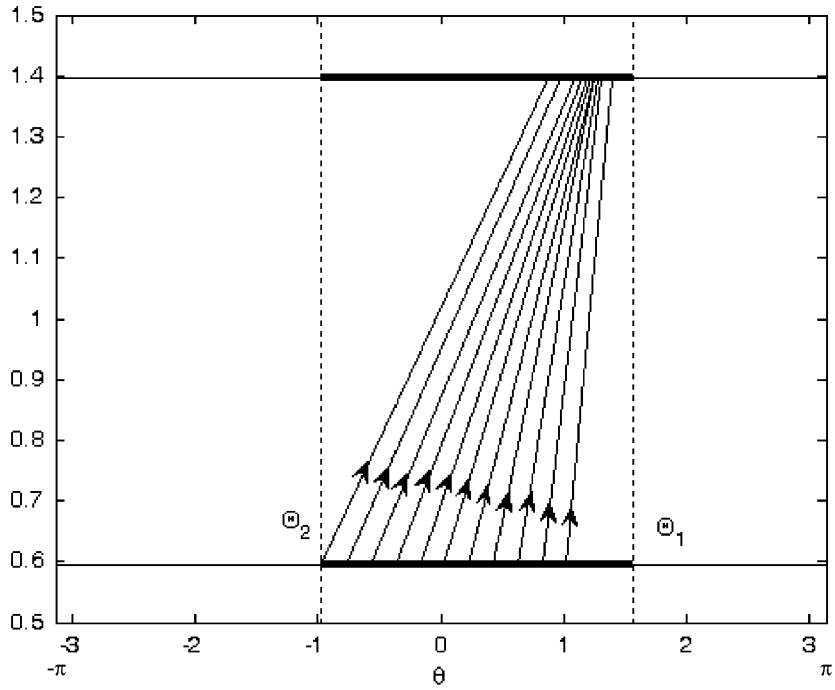

Fig. 16. One-dimensional mapping: $\sigma = -1.45$, $A_1 = 0.6$, $\lambda = 0.2$. Horizontal bold lines refer to the basin of jump $\Theta_1 < \theta < \Theta_2$, arrows denote direction of mapping.

4. Numerical verification

In the current section, numerical verifications of the analytical model are performed. Thus, for several values of frequency detuning parameters the amplitude of the response was calculated numerically via Runge–Kuta 4. Numerically obtained amplitudes are plotted together with the analytically derived frequency-response curves (Fig. 17). It is essential to note that numerical verification was done for the frequency-response diagram presented in Fig. 10.

Observing the diagram presented in Fig. 17, one can immediately notice that there is a frequency interval $\sigma = -1.25$, 1.6 for which SMR exists. In the current work, the interval of existence of the SMR was established analytically using the developed procedure of one-dimensional mapping diagrams. Thus, for various values of the frequency detuning parameter, mapping diagrams were constructed. All those diagrams, which constitute the contractive mapping suggest for the SMR existence when others suggest for the absence of it. Consequently, picking a small step size for frequency detuning variation we revealed a zone of SMR existence with the help of the one-dimensional mapping diagrams. In order to demonstrate the different types of regimes coexistence time-series diagrams were obtained for various values of the detuning parameter.

We start with $\sigma = 0.5$. According to the obtained frequency-response diagram in Fig. 17 for the selected value of frequency detuning we expect to observe the weakly quasiperiodic response (due to Hopf bifurcation) together with SMR. Time-series plots of this case are presented in Fig. 18.

Picking ($\sigma = 0.9$) one expects to obtain the coexistence of two system responses: periodic response and SMR as it comes from the diagram (Fig. 17). These responses are plotted in Fig. 19.

Additional frequency interval of interest is one for which there exist two distinct periodic responses together with SMR. In order to obtain the case of two periodic regimes coexistence together with SMR we have picked the value of σ which corresponds to the mentioned interval. Thus, picking ($\sigma = 1.5$) we have obtained numerically three distinct regimes presented in Fig. 20.

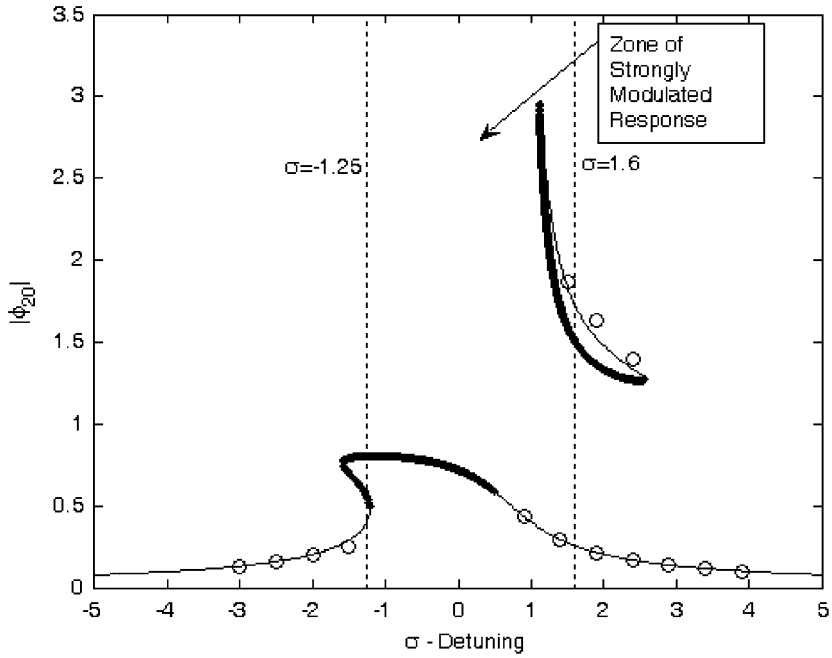

Fig. 17. Numerical verification of the frequency-response diagram: O—numerical integration, bold line—unstable periodic response, and thin solid line—stable periodic response.

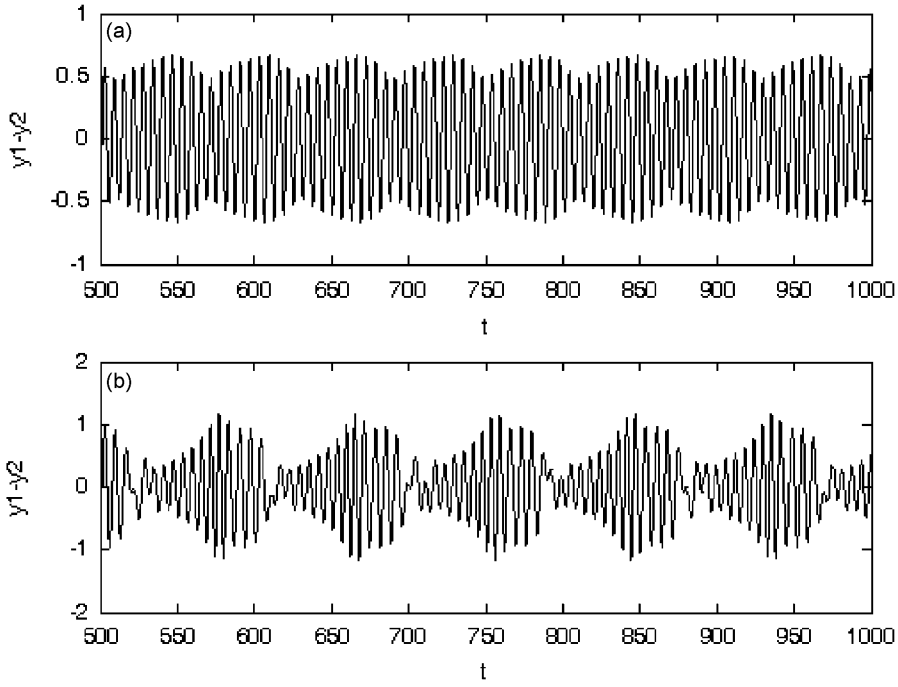

Fig. 18. The coexistence of two distinct responses: (a) weakly quasiperiodic response; (b) strongly modulated response; parameters: $A = 0.4$, $\lambda = 0.2$, $\sigma = 0.5$, $\varepsilon = 0.05$.

5. Concluding remarks

The detailed study of the simple periodic and quasiperiodic regimes occurring in the strongly nonlinear coupled system was performed in the work. Two types of local bifurcations of periodic solutions were

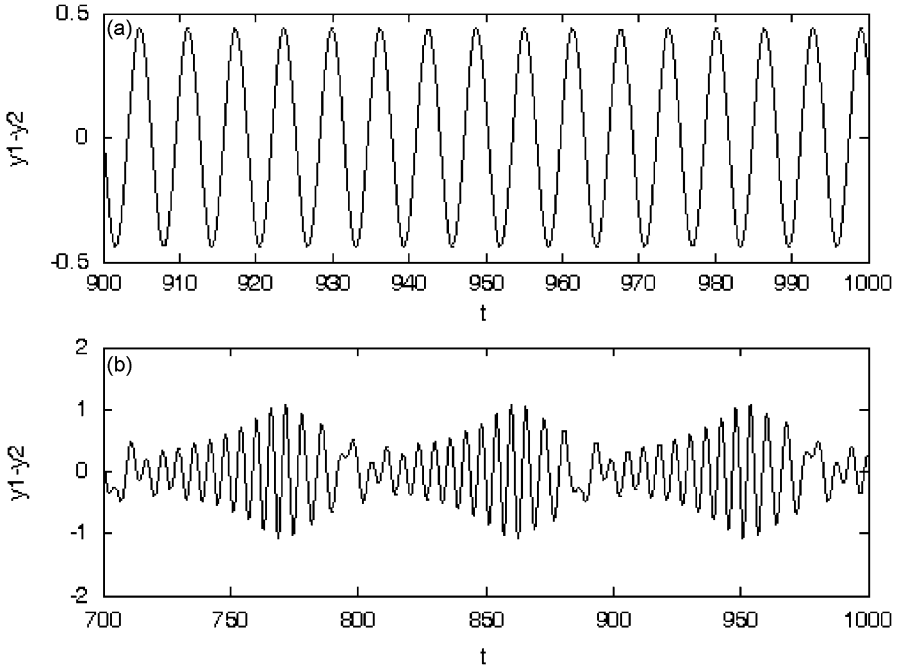

Fig. 19. The coexistence of two distinct responses: (a) weakly quasiperiodic response; (b) strongly modulated response; parameters: $A = 0.4$, $\lambda = 0.2$, $\sigma = 0.9$, $\varepsilon = 0.05$.

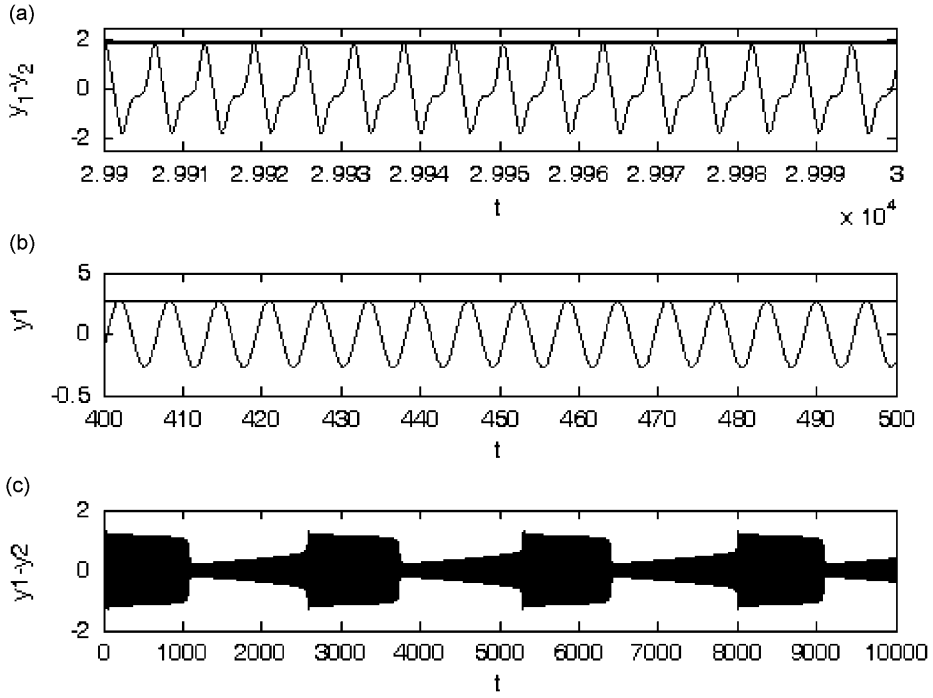

Fig. 20. The coexistence of three distinct responses: (a) periodic response with small amplitude; (b) periodic response with large amplitude; (c) the SMR; parameters: $A = 0.4$, $\lambda = 0.2$, $\sigma = 1.5$, $\varepsilon = 0.001$.

revealed. Periodic and quasiperiodic regimes were predicted analytically and verified numerically. Novel analytical approach for prediction of existence of SMR was presented in the paper. Zone of SMR was calculated via developed analytical approach. Various combinations of system regimes coexistence predicted by the analytical models were demonstrated numerically.

The most interesting case of the regimes combinations was a coexistence of three distinct regimes two of which are periodic and the third one is a SMR. Considerable agreement was observed between analytical model and numerical simulations.

Acknowledgment

The authors are very grateful to Israel Science Foundation (Grant 485/05) for financial support of this work.

References

[1] O.V. Gendelman, Transition of energy to nonlinear localized mode in highly asymmetric system of nonlinear oscillators, *Nonlinear Dynamics* 25 (2001) 237–253.
[2] O.V. Gendelman, A.F. Vakakis, L.I. Manevitch, R. McCloskey, Energy pumping in nonlinear mechanical oscillators I: dynamics of the underlying Hamiltonian system, *Journal of Applied Mechanics* 68 (1) (2001) 34–41.
[3] A.F. Vakakis, O.V. Gendelman, Energy pumping in nonlinear mechanical oscillators II: resonance capture, *Journal of Applied Mechanics* 68 (1) (2001) 42–48.
[4] A.F. Vakakis, Inducing passive nonlinear energy sinks in linear vibrating systems, *Journal of Vibration and Acoustics* 123 (2001) 324–332.
[5] A.F. Vakakis, L.I. Manevitch, O. Gendelman, L. Bergman, Dynamics of linear discrete systems connected to local essentially nonlinear attachments, *Journal of Sound and Vibration* 264 (2003) 559–577.
[6] O.V. Gendelman, Bifurcations of nonlinear normal modes of linear oscillator with strongly nonlinear damped attachment, *Nonlinear Dynamics* 37 (2004) 115–128.
[7] S.W. Shaw, C. Pierre, Normal modes for nonlinear vibratory systems, *Journal of Sound and Vibration* 164 (1993) 85–124.
[8] A.F. Vakakis, L.I. Manevitch, Y.V. Mikhlin, V.N. Pilipchuk, A.A. Zevin, *Normal Modes and Localization in Nonlinear Systems*, Wiley Interscience, New York, 1996.
[9] A.Jiang Xiaoai, M. McFarland, L.A. Bergman, A.F. Vakakis, Steady state passive nonlinear energy pumping in coupled oscillators: theoretical and experimental results, *Nonlinear Dynamics* 33 (2003) 7–102.
[10] O.V. Gendelman, E. Gourdon, C.H. Lamarque, Quasiperiodic energy pumping in coupled oscillators under periodic forcing, *Journal of Sound and Vibration* 294 (2006) 651–662.
[11] O.V. Gendelman, Y. Starosvetsky, Quasiperiodic response regimes of linear oscillator coupled to nonlinear energy sink under periodic forcing, *Journal of Applied Mechanics* 74 (2007) 325–331.
[12] O.V. Gendeman, Y. Starosvetsky, M. Feldman, Attractors of harmonically forced linear oscillator with attached nonlinear energy sink I: description of response regimes, *Nonlinear Dynamics* 51 (2008) 31–46.
[13] Y. Starosvetsky, O.V. Gendelman, Attractors of harmonically forced linear oscillator with attached nonlinear energy sink II: optimization of a nonlinear vibration absorber, *Nonlinear Dynamics* 51 (2008) 47–57.
[14] J. Guckenheimer, M. Wechselberger, L.-S. Young, Chaotic attractors of relaxation oscillators, *Nonlinearity* 19 (2006) 701–720.
[15] J. Guckenheimer, K. Hoffman, W. Weckesser, Bifurcations of relaxation oscillations near folded saddles, *International Journal of Bifurcations and Chaos* 15 (2005) 3411–3421.